1

2 **Chronic Benzene Exposure Aggravates Pressure Overload-Induced Cardiac Dysfunction**

3 Igor N. Zelko[1-4], Sujith Dassanayaka[2,4], Marina V. Malovichko[1-4], Caitlin M. Howard[2-4], Lauren

4 F. Garrett[2-4], Uchida Shizuka[1-3], Kenneth R. Brittian[2-4], Daniel J. Conklin[1-4], Steven P. Jones[2-4] and

5 Sanjay Srivastava[1-4]

6

7 [1]University of Louisville Superfund Research Center, [2]Diabetes and Obesity Center, [3]Envirome
8 Institute, and [4]Department of Medicine, Division of Environmental Medicine, University of
9 Louisville, Louisville, KY 40202

10

11 Running Title: Benzene-induced cardiac dysfunction
12
13
14 Conflict of interest statement: The authors have declared that no conflict of interest exists
15
16
17
18 Address correspondence to: Igor N. Zelko, PhD
19 Department of Medicine
20 Division of Environmental Medicine
21 Room 310 CII Building
22 302 E. Muhammad Ali Blvd
23 Louisville, KY 40202
24 Phone: 502-852-9064
25 E-mail: igor.zelko@louisville.edu
26
27 or
28
29 Sanjay Srivastava, PhD
30 Superfund Research Center,
31 Room 306 CII Building
32 302 E. Muhammad Ali Blvd
33 Louisville, KY 40202
34 Phone: 502-852-5724; Fax: 502-852-5834
35 E-mail: sanjay@louisville.edu

ABSTRACT

Benzene is a ubiquitous environmental pollutant abundant in household products, petrochemicals and cigarette smoke. Benzene is a well-known carcinogen in humans and experimental animals; however, little is known about the cardiovascular toxicity of benzene. Recent population-based studies indicate that benzene exposure is associated with an increased risk for heart failure. Nonetheless, it is unclear whether benzene exposure is sufficient to induce and/or exacerbate heart failure. We examined the effects of benzene (50 ppm, 6 h/day, 5 days/week, 6 weeks) or HEPA-filtered air exposure on transverse aortic constriction (TAC)-induced pressure overload in male C57BL/6J mice. Our data show that benzene exposure had no effect on cardiac function in the Sham group; however, it significantly compromised cardiac function as depicted by a significant decrease in fractional shortening and ejection fraction, as compared with TAC/Air-exposed mice. RNA-seq analysis of the cardiac tissue from the TAC/benzene-exposed mice showed a significant increase in several genes associated with adhesion molecules, cell-cell adhesion, inflammation, and stress response. In particular, neutrophils were implicated in our unbiased analyses. Indeed, immunofluorescence studies showed that TAC/benzene exposure promotes infiltration of CD11b$^+$/S100A8$^+$/myeloperoxidase$^+$-positive neutrophils in the hearts by 3-fold. *In vitro*, the benzene metabolites, hydroquinone and catechol, induced the expression of P-selectin in cardiac microvascular endothelial cells by 5-fold and increased the adhesion of neutrophils to these endothelial cells by 1.5-2.0-fold. Benzene metabolite-induced adhesion of neutrophils to the endothelial cells was attenuated by anti-P-selectin antibody. Together, these data suggest that benzene exacerbates heart failure by promoting endothelial activation and neutrophil recruitment.

Keywords: Benzene, heart failure, adhesion molecules, endothelial cells, neutrophils, RNA-seq.

2

Introduction

Environmental pollution is a health problem worldwide. More than 9 million premature deaths are attributed to pollution every year, out of which 6 million deaths are related to air pollution (1). Nearly half of the air pollution-associated deaths are ascribed to cardiovascular disease (1). Cardiovascular health effects of criteria pollutants (particulate matter$_{2.5}$, sulfur dioxide, carbon monoxide, nitrogen oxides, ozone and lead) have been extensively studied in the last three decades; however, information about the potential cardiovascular toxicity of other airborne chemicals, such as volatile organic compounds (e.g. benzene, 1,3-butadiene, vinyl chloride, trichloroethylene etc.), is sparse. Benzene, a well-known carcinogen, is abundant in household products, cigarette smoke and automobile exhaust (2-5), and the atmospheric concentration of benzene can exceed 50 ppm, especially near the emission source. People working at gasoline pumping stations or living near hazardous waste sites can be exposed to high levels of benzene. The United States Occupational Safety and Health Administration has set the occupational benzene exposure limit of 1 ppm (6); however, occupational benzene exposure in excess of 100 ppm has been reported in developing countries (7).

Like pollution, heart failure is a pervasive health problem. Heart failure affects more than 6.5 million people in the United States (8) and 26 million people worldwide (9). The lifetime risk for heart failure at 40 years of age is estimated to be 1 in 5 people (10). The pathogenesis of heart failure is also not clearly understood, although a substantial body of literature points to the important role of infiltrating immune cells in the development of left ventricular hypertrophy and cardiac dysfunction (11-18). Therefore, the current focus in finding new therapeutic approaches to delay advanced heart failure includes understanding the molecular mechanisms that govern cardiomyocyte interactions with immune cells (19-21). The innate immune response induced by heart failure initiates the cardiac repair process, and involves infiltration of peripheral neutrophils (22-24).

Recent population based studies have reported that benzene exposure is associated with an increased risk for heart failure (25), and presence of mono-nitrogen oxide and benzene in the air of hospital wards is associated with a higher risk of heart failure morbidity (26). Other studies have linked exposure to benzene with cardiovascular mortality (27, 28); however, direct effects of

3

90   benzene exposure on heart failure in well-controlled animal studies have not been studied. Here,

91   we examined the effect of chronic benzene exposure on transverse aortic constriction (TAC)-

92   induced cardiac function and associated immune response in mice.

93

94   **MATERIALS AND METHODS**

95

96   **Reagents:** Benzene permeation tubes were obtained from Kin-Tek (La Marque, TX). Primers and

97   probes for real-time PCR were purchased from Integrated DNA Technologies (Coralville, IA) and

98   ThermoFisher Scientific (Waltham, MA). Sources of antibodies used for immunohistochemistry

99   and functional studies were: anti-CD11b, myeloperoxidase (Abcam); anti-S100A8 (63N13G5)-

100   FITC from Novus (Novus, Centennial, CO); anti-CD90/Thy1 from Sino Biological (Sino

101   Biological); CD62P from Biolegend (San Diego, CA). Murine cardiac microvascular endothelial

102   cells (CMVEC) were obtained from CellBiologics, Chicago, IL. All other chemicals and enzymes

103   were from Sigma Chemical Co. (St. Louis, MO), or Invitrogen (Carlsbad, CA).

104

105   **Animal housing and maintenance:** C57BL/6J male mice obtained from Jackson Laboratory (Bar

106   Harbor, ME) were maintained on normal chow in a pathogen-free facility accredited by the

107   Association for Assessment and Accreditation of Laboratory Animal Care. All procedures were

108   approved by the University of Louisville Institutional Animal Care and Use Committee.

109

110   **Animal Surgeries:** For TAC (29), male C57BL/6J mice 12 weeks of age were anesthetized

111   (intraperitoneal injections of 50 mg/kg sodium pentobarbital and 50 mg/kg ketamine

112   hydrochloride), antiseptically prepared for surgery, orally intubated, and ventilated (oxygen

113   supplement to the room-air inlet) with a mouse ventilator (Hugo Sachs). Core body temperature

114   was maintained at 36.5–37.5°C with an automatic, electronically regulated heat lamp. The aorta

115   was visualized following an intercostal incision. A 7-0 nylon suture was looped around the aorta

116   between the brachiocephalic and left common carotid arteries. The suture was tied around a 27-

117   gauge needle placed adjacent to the aorta to constrict the aorta to a reproducible diameter. The

118   needle was removed, and the chest was closed in layers. Mice were extubated upon recovery of

119   spontaneous breathing. Analgesia (ketoprofen, 5 mg/kg) was provided prior to recovery and by 24

120   and 48 h post-surgery. Sham mice were subjected to the same procedure as the TAC cohort except

121   the suture was not tied.

122

123   **Benzene Exposure:** One week after the TAC, mice were exposed to benzene for 6 weeks in

124   bedding-free cages as described before (30). Briefly, benzene atmospheres were generated from

125   liquid benzene (Sigma-Aldrich) in a KIN-TEK Analytical, Inc permeation tube. A carrier gas (N_2)

126   was delivered to the permeation tube at 100 ml/min and diluted with HEPA- and charcoal-filtered

127   room air (3 L/min) and diluted gas directed to an exposure unit. Flow was distributed through a

128   fine mesh screen of a custom cyclone-type top (Teague Enterprises) that distributed air within 10%

129   of the mean concentration at six locations in the cage. Throughout the exposure, benzene

130   concentrations were continuously monitored using an in-line photoionization detector (ppb RAE:

131   Rae Industries) upstream of the exposure unit. Mice were exposed to 50 ppm benzene (6 h/day, 5

132   days/week) for 6 weeks. Mice exposed to HEPA- and charcoal-filtered room air only were used as

133   controls.

134

135   **Echocardiography:** At the end of the benzene exposure protocol, mice were anesthetized with

136   2% isoflurane, and echocardiography was performed (VisualSonics Vevo 3100), similar to our

137   previous reports (29, 31). At the end of the experiment, hearts were excised for biochemical and

138   pathological analyses. For mice in the TAC arm of the study, Doppler verification of the stenosis

139   was used. The sonographer was blinded to the specific experimental group.

140

141   **RNA Isolation and RNAseq analysis:** Total RNA was extracted from the hearts of mice using

142   TRIzol kit (Thermo Fisher Scientific, MA, USA), and the purity of RNA was analyzed using

143   NanoDrop One (ThermoScientific, MA, USA). RNA quality was measured by Agilent 2100

144   bioanalyzer (Thermo Fisher Scientific, MA, USA) and samples with high RNA integrity were used

145   for subsequent RNAseq analysis. RNA samples were processed by Novogene using mRNA and

146   small RNA sequencing services (Novogene, Beijing, China). The resultant raw reads of the

147   FASTQ files were processed and quality metrics were visualized using FastQC v 0.11.9. The

148   mRNA differentially regulated genes (DEG) and pathway enrichment analysis were performed

149   using the NGS Data Analysis pipeline (32).

150

Histopathology: Formalin-fixed, paraffin-embedded hearts from Sham and TAC mice were sectioned at 4 μm thickness, and later deparaffinized, and rehydrated according to the appropriate staining method. The histological staining was performed as previously described (33, 34). Picro-Sirius Red staining was used to evaluate tissue fibrosis and general histology, and Alexa Fluor 555-conjugated wheat-germ agglutinin (Invitrogen) staining was used to determine the average myocyte area. All images were captured at 20X magnification using the Keyence BZ-X810, all in one fluorescent microscope. Both fibrosis and myocyte area were analyzed using the hybrid cell count feature (BZ-H4C) associated with the Keyence system. Fibrosis was expressed as a percentage of scar tissue divided by the total area of tissue.

Immunofluorescence: For immunostaining, deparaffinized and rehydrated sections were incubated for 20 min with 10 mmol/L citric acid pH 6.0 (pH 9.0 for MPO staining). Nonspecific binding was blocked with 5% normal goat serum and 0.05% saponin (Sigma) in PBS (pH 7.4) for 30 min. Sections were blocked and then incubated with the appropriate primary antibody in PBS with 1% BSA and 0.05% saponin for 1 h at 37°C against: CD11b (Abcam), S100A8-FITC (Novus), myeloperoxidase (Abcam). Tissue sections were then incubated for 30 min at room temperature with respective secondary antibodies conjugated with Alexa 488, 555, or 647 (Invitrogen), and counterstained with DAPI to label nuclei. Images were made with a 20x and 60x objective.

Neutrophils isolation: Neutrophils were isolated from bone marrow as described previously (35). Briefly, C57BL6/J male mice 10 weeks old were sacrificed using pentobarbital injection. Bone marrow cells were flushed from the femur and tibia and filtered through a 70 μm mesh filter. For a negative selection of neutrophils, we used a Neutrophil Isolation kit from Miltenyi, Auburn, CA. Magnetic sorting was performed using MS columns. Neutrophils presented in flow-through fractions were characterized using flow cytometry and by cytospin with Diff-Quick staining. Neutrophil purity was always higher than 93%.

Cell adhesion assay: Neutrophil adhesion to CMVEC was determined as previously described (36). Briefly, CMVEC (passage 6 to 10) were seeded into 96-well plate at 25,000 cells per well in 100 μl of growth media. Twenty-four hours later confluent monolayer of endothelial cells was

182   exposed to benzene metabolite catechol (5 µM) for 24 hours. Cells treated with TNFα (100 ng/mL)

183   for 4 hours served as positive controls. Isolated neutrophils labeled with calcein (36) were added

184   to endothelial cells and incubated for 30 min at 37 $^{\circ}$C. Cells were rinsed with PBS containing Mg^{2+}

185   and Ca^{2+} and the fluorescence was measured with a Synergy H1 (Biotek) fluorescence plate reader

186   (excitation wavelength, 485 nm and emission wavelength, 520 nm). To measure the effect of p-

187   selectin blocking on neutrophil adhesion, CMVEC were incubated with anti-CD62P antibodies

188   (25 µg/mL) for 30 min prior to the neutrophil adhesion assay. For each assay, 10-12 wells were

189   used.

190

191   **Statistical Analyses:** Data are presented as means ± SEM. The statistical significance of

192   differences was determined by t-test. A one-way analysis of variance (ANOVA) with Holm-Sidak

193   *post hoc* test was used to compare differences between multiple treatment groups. P-value of <0.05

194   indicated statistically significant differences. All analyses were performed using Excel and

195   GraphPad Prism software (GraphPad Software, San Diego, CA). Statistical analyses for echo-

196   based parameters were performed after adjustment for body weight and heart rate by two-way

197   ANOVA with Tukey-Kramer corrections.

198

199   **RESULTS**

200   **Benzene exposure exacerbates pressure overload-induced cardiac dysfunction:** As expected,

201   mice in the TAC/Air group developed significant left ventricular dilation as indicated by a

202   significant increase in end diastolic volume (EDV), end systolic volume (ESV) and left ventricular

203   internal diameter in diastole (LVIDd), and diameter in systole (LVIDs), and consequent decrease

204   in fractional shortening (FS) and ejection fraction (EF), as compared with the mice in

205   corresponding Sham/Air (**Fig. 1**). TAC also increased the heart mass, cardiac myocyte size and

206   fibrosis in the heart (**Fig. 1**). This was accompanied with a significant increase in the fluid

207   accumulation in the lung (**Supplemental Fig. 1**). Benzene exposure had no effect on myocyte size

208   and cardiac function in the Sham group; however, it significantly compromised cardiac function

209   as depicted by a significant increase in EDV, ESV, LVIDd, and LVIDs and resultant decrease in

210   FS and EF, as compared with TAC/Air-exposed mice (**Fig. 1** and ***Supplemental* Table 1**). The

211   other cardiac function parameters such as left ventricular anterior wall thickness at diastole or

212   systole (LVAWd and LVAWs) and left ventricular posterior wall thickness at diastole or systole

213   (LVPWd and LVPWs), isovolumic relaxation time (IVRT), Stroke Volume (SV), and Cardiac

214   Output (CO) did not significantly change in TAC/Benzene vs TAC/Air groups (***Supplemental***

215   ***Table 1***). Cardiac myocyte size and fibrosis in TAC/Benzene-exposed mice were also comparable

216   with the TAC/Air-exposed mice. Collectively, these data suggest that a 6-week benzene exposure

217   exacerbates TAC-induced cardiac dysfunction but does not induce cardiac remodeling in Sham

218   mice.

219

220   **RNA-Seq analyses of TAC-benzene-exposed hearts:** To examine the molecular mechanisms by

221   which benzene worsens cardiac function following TAC, we performed deep RNA sequencing on

222   the left ventricle and septum tissues. For these analyses, we used FDR ≤ 0.01 and 0.5 ≤ Log2 (fold

223   change) ≤ -0.5 to examine the differential expression of the genes. As shown in **Fig 2A**, TAC

224   upregulated 671 genes (e.g., genes involved in extracellular matrix organization and collagen

225   formation) and downregulated 351 genes (e.g., genes involved in muscle contraction and cardiac

226   conduction) in the air-exposed mice (see ***Supplemental Table 1***). Exposure to benzene in Sham-

227   operated mice did not induce any genes while uteroglobin (*Scgb1a1*) and surfactant protein C

228   (*Sftpc*) were downregulated by 8.9- and 6.1-fold. However, benzene exposure in TAC mice

229   significantly upregulated 876 genes and downregulated 674 genes as compared with the

230   corresponding Sham-operated controls. Comparison of the gene expression between

231   TAC/Benzene versus TAC/Air mice showed upregulation of 50 and downregulation of 69 genes.

232   **Fig. 2B** illustrates the heat-map of top the 15 upregulated and 10 downregulated genes between

233   these groups as well as the differential expression of these genes in the other experimental groups.

234   Gene ontology of biological process and molecular function enrichment analyses of differentially

235   expressed genes in the benzene-exposed TAC hearts show significant enrichment of the genes

236   associated with the regulation of "neutrophil degranulation", "signaling by interleukins",

237   "extracellular matrix organization", "platelet degranulation", and heat shock factor-1 (HSF-1) -

238   dependent transactivation etc. (**Fig. 3A**). **Fig. 3B** shows the induction of some representative genes

239   of these processes, and **Fig. 3C** displays the gene-concept network of select differentially

240   expressed genes associated with the indicated biological pathways including neutrophil

241   degranulation, interleukin signaling, and HSF-1 activation.

242

Benzene exposure augments TAC-induced neutrophil infiltration: Because our RNA-Seq data suggest that benzene exposure affects inflammatory response and neutrophil degranulation processes in TAC hearts, we examined the abundance of inflammatory cells in the TAC/benzene-exposed hearts. As shown in **Fig. 4A**, benzene exposure induced massive infiltration of S100A8-positive granulocytes in the hearts of TAC mice. These cells also co-stained with the pan-myeloid marker CD11b and myeloperoxidase, mostly expressed on neutrophils (**Fig. 4A and 4B**). Quantitative analysis shows >3-fold increase in S100A8$^+$ granulocytes, CD11b$^+$ myeloid cells and myeloperoxidase$^+$ neutrophils in TAC/Benzene vs TAC/Air groups (**Fig. 4C**). The S100A8 staining did not co-localize with the markers of CD68$^+$ macrophages and Thy1$^+$ fibroblasts in TAC-Benzene hearts (***Supplemental* Fig. 2**). To examine the mechanisms by which benzene exposure augments neutrophil infiltration in TAC-instrumented hearts, we analyzed the RNA-seq data for the differential expression of adhesion molecules. As shown in **Fig. 4D**, benzene exposure did not affect the levels of adhesion molecules in the Sham-operated hearts, however, it significantly increased the transcription of Intracellular adhesion molecule-1 (*Icam1*), endothelial-selectin (*Sele*), and platelet-selectin (*Selp*) genes in the TAC-instrumented hearts. Expression of vascular cell adhesion molecule (*Vcam1*) in TAC-benzene hearts was comparable with the TAC/Air hearts. Together, these data indicate that chronic benzene exposure enhances the infiltration of neutrophils, possibly by activating adhesion molecules in the myocardial endothelial cells during pressure overload-induced cardiac dysfunction.

P-Selectin facilitates the adhesion of neutrophils adhesion to the cardiac microvascular endothelial cells: Complimentary *in vitro* experiments with CMVEC showed that benzene metabolites hydroquinone (5 μM, 24 h) and catechol (5 μM, 24 h) increased the transcription of P-selectin by 5-fold (**Fig. 5A**) and abundance of P-selectin protein by 1.5-2-fold (**Fig. 5B**). Incubation of CMVEC with catechol for 24 h augmented the adhesion of bone marrow-derived neutrophils to CMVEC (**Fig. 5C**), which was attenuated by pre-incubation of CMVEC with anti-P-selectin antibody (**Fig. 5D**). Hydroquinone and catechol also increased the expression of interleukin-8 (IL8, ***Supplemental* Fig. 3**), which can function both as a membrane-bound and soluble activator of neutrophil β2 integrin-mediated adhesion. Together, these observations suggest that benzene-induced neutrophil infiltration in the TAC hearts could be facilitated, at least in part, by the metabolic conversion of benzene to its active metabolites- hydroquinone and catechol.

9

DISCUSSION

The major finding of this study is that chronic benzene exposure exacerbates pressure overload-induced cardiac dysfunction. The TAC/Benzene-induced cardiac dysfunction is accompanied by endothelial activation and enhanced recruitment of granulocytes in the heart and differential regulation of genes involved in neutrophil degranulation, inflammatory signaling, and stress response. These studies corroborate recent reports that occupational and environmental exposure to benzene is associated with an increased risk for heart failure (25).

Inflammatory processes have long been implicated in the manifestation, progression, and consequences of ischemic heart disease (37, 38) and pressure- or volume overload-induced mechanical stress (17, 39-41). Pressure overload induces the expression of *ICAM1* (42) and consequent increase in the recruitment of neutrophils in the heart (39) and subsequent monocyte infiltration (17, 39). It diminishes TAC-induced cardiac hypertrophy and inflammation and sustains cardiac function (39), suggesting that neutrophils play a pivotal role in the manifestation of heart disease, especially heart failure. In mice, increased recruitment of S100A9 positive granulocytes, which co-stained with myeloperoxidase, suggests that TAC/Benzene exposure facilitates the infiltration of neutrophils into the hearts.

This is further supported by RNAseq data of cardiac tissue, demonstrating robust induction in the neutrophil specific *S100A8/A9*, *Mmp8*, *Lcn2*, and *Cxcr2* transcripts. S100A8/A9 is a member of alarmins or damage-associated molecular patterns (DAMPs) that are released by the failing heart (43-45) and subsequently activate resident macrophages, fibroblasts, and endothelial cells to secrete proinflammatory cytokines and adhesion molecules (46) and augment inflammation in the cardiac tissue (21, 23, 47). Systemic administration of S100A8/A9 facilitates the mobilization of neutrophils from the bone marrow (48) while local administration of S100A8/A9 leads to rapid recruitment of monocytes and neutrophils into the site of injury (49). Patients with myocardial infarction and elevated S100A8/A9 levels have poorer prognosis (50, 51). Overall, increased neutrophil infiltration in the hearts could play a pivotal role in benzene exposure-induced cardiac dysfunction in the pressure overload hearts.

Although precise mechanisms by which benzene exposure exacerbates pressure overload-induced cardiac dysfunction remain unknown, it is plausible that the observed enlargement of left ventricle

10

304 dimensions in the hearts of TAC/Benzene mice could, at least in part, be due to the induction of
305 neutrophil gelatinase-associated lipocalin (NGAL or Lcn2) whose expression is regulated by the
306 S100A8/A9 complex (52). Lcn2 plays a central role in the ontogeny of cardiac hypertrophy and
307 heart failure (53-55) and can bind Mmp9 to create a complex to stabilize Mmp9 protein and
308 enhance metalloproteinase activity with its pro-angiogenic and pro-invasive properties (56, 57).
309 Moreover, S100A8/A9 can diminish cardiac myocyte contractility, resulting in attenuated cardiac
310 ejection fraction (58). Patients of chronic heart failure have elevated plasma myeloperoxidase
311 levels (59), and pharmacological inhibition of myeloperoxidase diminishes leukocyte recruitment,
312 and improves ejection fraction, end diastolic/systolic volume, and left ventricular hypertrophy
313 following myocardial infarction (60). Therefore, it is conceivable that the augmented neutrophil
314 infiltration with subsequent release of MPO and S100A8/A9 heterodimer from activated
315 granulocytes might affect myocyte contractility and compromise cardiac function in TAC/Benzene
316 mice.

317 Increased inflammation in the hearts of mice subjected to pressure overload followed by benzene
318 exposure is further underscored by the increased transcription of chemokines, cytokines, and their
319 receptors (e.g. Il1β, Cxcl1, and Cxcr2). Chemokines such as CXCL1 chemokine are well known
320 to facilitate neutrophil migration into inflamed tissues (61), promote angiogenesis (62, 63) and
321 regulate the recruitment of neutrophils and monocytes during cardiac remodeling and
322 inflammation (64). Although the cellular sources (e.g., endothelial cells, granulocytes) of CXCL1
323 and other chemokines and cytokines in the hearts of TAC/benzene-exposed mice remain unknown,
324 they likely augment neutrophil recruitment and migration. Benzene metabolites have been shown
325 to increase the expression of cytokines and chemokines in the peripheral blood mononuclear cells
326 (65) and endothelial cells (66). Our *in vitro* studies show that in murine cardiac microvascular
327 endothelial cells, benzene metabolites hydroquinone and catechol increase the transcription of
328 chemokine IL-8, which is known to bind to CXCR2 on neutrophils and trigger a signaling cascade
329 that facilitates a firm monocyte adhesion with subsequent intravasation (67). Further studies are
330 required to delineate the sources of chemokines and cytokines and the molecular mechanisms by
331 which these molecules promote inflammatory signaling in the hearts of TAC/Benzene mice.

332 Induction of heat shock proteins (HSPs) such as *Hspa1a* and *Hspa1b* in Sham/Benzene hearts
333 appears to be an adaptive response to circumvent inflammatory signaling. Induction of HSPs in
334 response to chemical and mechanical stress enhances protein folding, inhibits inflammation and

11

335 apoptosis, and provides cytoskeletal protection (68). While little is known about the role of HSPs

336 in pressure overload-induced heart failure, heat shock factor 1 (HSF-1), the transcription factor

337 that regulates HSPs is induced by TAC in rats and mice, and constitutive activation of HSF-1

338 ameliorates TAC-induced cardiac hypertrophy, fibrosis and cardiac dysfunction (69-71).

339 Conversely, inhibition of HSF-1 impairs cardiac function in the pressure overload subjected hearts

340 (69, 70). The HSF-1-mediated cardiac adaptation from pressure overload has been attributed, at

341 least in part, to myocardial angiogenesis via suppression of p53 and subsequent induction of HSF-

342 1 (72). HSF-1 can also improve endothelial function (73) and prevent inflammatory signaling (74).

343 Although the contribution of the HSF-1/HSP axis in the etiology of cardiac dysfunction following

344 TAC/Benzene exposure is unclear, it is likely that these pathways are activated to prevent benzene-

345 induced endothelial activation. Further studies are required to examine the molecular mechanisms

346 by which HSF-1-dependent transactivation prevents endothelial activation.

347 Collectively, our studies demonstrate that benzene exposure worsens pressure overload-induced

348 cardiac dysfunction, which is accompanied by increased influx of neutrophils, alterations in cell-

349 cell adhesion, and induction of genes associated with inflammation and stress response. These

350 studies establish the plausibility that benzene exposure is sufficient to exacerbate TAC-induced

351 cardiac dysfunction and provide insight about the underlying mechanisms.

352

357

358

359

360

361

362

363   FIGURE LEGENDS:

364   **Figure 1.** *Effect of benzene exposure on left ventricle function and cardiac remodeling after*

365   *pressure overload.* **A.** Benzene exposure protocol: Transverse aortic constriction or Sham operated

366   male C57BL/6 mice were exposed to benzene (50 ppm, 6 h/day, 5 days/week) or HEPA-filtered

367   air (Air) for 6 weeks. At the end of the exposure protocol, echocardiography was used to measure

368   ejection fraction (**B**), fractional shortening (**C**), end-diastolic volume (EDV; **D**), end-systolic

369   volume (ESV; **E**), left ventricular internal diameter end diastole (LVIDd; **F**) and end systole

370   (LVIDs; **G**). Heart weight:tibial length (TL) are presented in panel **H**. Panel **I** shows the

371   representative images of Sirius Red-stained mid-ventricular histological sections from mouse

372   hearts with quantitative analysis of fibrosis expressed as percent of fibrous area to total area ratio.

373   Representative images of wheat germ agglutinin (WGA)-stained mid-ventricular histological

374   sections from mouse hearts with quantitative analysis of myocyte area are illustrated in panel **J**.

375   Values are mean ± SEM. *p<0.05, **p<0.01, ***p<0.001, and ****p<0.0001 represent statistical

376   significance between corresponding groups analyzed by One-way ANOVA. N=6-11/group.

377

378   **Figure 2.** *Differential expression of genes (DEG) in the hearts of TAC/Benzene-exposed mice.*

379   **A.** The number of differentially expressed genes (DEG) are depicted by corresponding arrows.

380   The visual representation of DEG for three treatments are presented as volcano plots (FDR ≤ 0.01).

381   **B**. Heatmap of the top 15 up-regulated and 10 down-regulated (TAC/Benzene vs. TAC/Air)

382   protein-encoding genes in the four experimental groups.

383

384   **Figure 3.** *Pathway enrichment analysis of differentially expressed genes in the hearts of*

385   *TAC/Benzene-exposed mice.* **A.** Dot plot of enriched terms for TAC/Benzene vs TAC/Air DEG

386   (FDR ≤ 0.01). IGF – Insulin-like Growth Factor, IGFBPs – Insulin-like Growth Factor Binding

387   Proteins; **B.** The most upregulated and functionally important genes in TAC/Benzene vs TAC/Air

388   groups. **C.** Gene-concept network depicting the linkage of genes and enriched biological pathways

389   as a network.

390

391   **Figure 4.** *Immune cells infiltration into the heart of TAC/Benzene-exposed mice.* **A.** Heart

392   sections were stained for S100A8 (green) and CD11b (pink), nuclei (blue); **B.** Co-staining of

393   S100A8 positive cells with myeloperoxidase (MPO) positive cells. **C.** Quantitative analysis of

13

394   S100A8-, CD11b-, and MPO-positive cells. **D.** Expression levels of adhesion genes in the hearts

395   of exposed mice. Values are mean ± SEM. *p<0.05, **p<0.01 and ***p<0.001 represent statistical

396   significance between corresponding groups analyzed by One-way ANOVA. N=6/group.

397

398   **Figure 5.** *Benzene metabolites induce neutrophil adhesion to the cardiac microvascular*

399   *endothelial cells*. **A.** Transcription of P-selectin (*Selp*) in cardiac microvascular endothelial cells

400   (CMVEC) treated with benzene metabolites hydroquinone (HQ; 5 µM, 6 h) and catechol (5 µM,

401   24 h). **B.** HQ (5 µM, 24 h)- and catechol (5 µM, 24 h)-induced upregulation of P-selectin protein

402   in CMVEC. **C.** Adhesion of bone marrow-derived calcein-labeled murine neutrophils to CMVEC

403   pretreated with HQ (5 µM) and Catechol (5 µM) for 24 hours. **D.** Inhibition of neutrophil adhesion

404   to HQ (5 µM, 24 h)- and catechol (5 µM, 24 h)-stimulated CMVEC by anti-P-selectin antibody.

405   Values are mean ± SEM. *p<0.05, **p<0.01, ***p<0.001, and ****p<0.0001 between

406   corresponding groups analyzed by One-way ANOVA.

407

408

409

410

411

412

413

414

415

416

417

418

419

420

421

REFERENCES

1. Collaborators, G.B.D.R.F. (2016) Global, regional, and national comparative risk assessment of 79 behavioural, environmental and occupational, and metabolic risks or clusters of risks, 1990-2015: a systematic analysis for the Global Burden of Disease Study 2015. *Lancet.* **388**(10053): p. 1659-1724.

2. Clayton, C.A., E.D. Pellizzari, R.W. Whitmore, R.L. Perritt, and J.J. Quackenboss (1999) National Human Exposure Assessment Survey (NHEXAS): distributions and associations of lead, arsenic and volatile organic compounds in EPA region 5. *J Expo Anal Environ Epidemiol.* **9**(5): p. 381-392.

3. Fraser, M.P., G.R. Cass, and B.R.T. Simoneit (1998) Gas-phase and particle-phase organic compounds emitted from motor vehicle traffic in a Los Angeles roadway tunnel. *Environmental Science & Technology.* **32**(14): p. 2051-2060.

4. Jacob, P., 3rd, A.H. Abu Raddaha, D. Dempsey, C. Havel, M. Peng, L. Yu, and N.L. Benowitz (2013) Comparison of nicotine and carcinogen exposure with water pipe and cigarette smoking. *Cancer Epidemiol Biomarkers Prev.* **22**(5): p. 765-772.

5. Appel, B.R., G. Guirguis, I.S. Kim, O. Garbin, M. Fracchia, C.P. Flessel, K.W. Kizer, S.A. Book, and T.E. Warriner (1990) Benzene, benzo(a)pyrene, and lead in smoke from tobacco products other than cigarettes. *Am J Public Health.* **80**(5): p. 560-564.

6. Smith, M.T. (2010) Advances in understanding benzene health effects and susceptibility. *Annu Rev Public Health.* **31**: p. 133-148 132 p following 148.

7. Wong, O. and H. Fu (2005) Exposure to benzene and non-Hodgkin lymphoma, an epidemiologic overview and an ongoing case-control study in Shanghai. *Chem Biol Interact.* **153-154**: p. 33-41.

8. Benjamin, E.J., M.J. Blaha, S.E. Chiuve, M. Cushman, S.R. Das, R. Deo, S.D. de Ferranti, J. Floyd, M. Fornage, C. Gillespie, C.R. Isasi, M.C. Jimenez, L.C. Jordan, S.E. Judd, D. Lackland, J.H. Lichtman, L. Lisabeth, S. Liu, C.T. Longenecker, R.H. Mackey, K. Matsushita, D. Mozaffarian, M.E. Mussolino, K. Nasir, R.W. Neumar, L. Palaniappan, D.K. Pandey, R.R. Thiagarajan, M.J. Reeves, M. Ritchey, C.J. Rodriguez, G.A. Roth, W.D. Rosamond, C. Sasson, A. Towfighi, C.W. Tsao, M.B. Turner, S.S. Virani, J.H. Voeks, J.Z. Willey, J.T. Wilkins, J.H. Wu, H.M. Alger, S.S. Wong, P. Muntner, C. American Heart Association Statistics, and S. Stroke Statistics (2017) Heart Disease and Stroke Statistics-2017 Update: A Report From the American Heart Association. *Circulation.* **135**(10): p. e146-e603.

9. Ponikowski, P., S.D. Anker, K.F. AlHabib, M.R. Cowie, T.L. Force, S. Hu, T. Jaarsma, H. Krum, V. Rastogi, L.E. Rohde, U.C. Samal, H. Shimokawa, B. Budi Siswanto, K. Sliwa, and G. Filippatos (2014) Heart failure: preventing disease and death worldwide. *ESC Heart Fail.* **1**(1): p. 4-25.

10. Lloyd-Jones, D.M., M.G. Larson, E.P. Leip, A. Beiser, R.B. D'Agostino, W.B. Kannel, J.M. Murabito, R.S. Vasan, E.J. Benjamin, D. Levy, and S. Framingham Heart (2002) Lifetime risk for developing congestive heart failure: the Framingham Heart Study. *Circulation.* **106**(24): p. 3068-3072.

11. Kain, D., U. Amit, C. Yagil, N. Landa, N. Naftali-Shani, N. Molotski, V. Aviv, M.S. Feinberg, O. Goitein, T. Kushnir, E. Konen, F.H. Epstein, Y. Yagil, and J. Leor (2016) Macrophages dictate the progression and manifestation of hypertensive heart disease. *Int J Cardiol.* **203**: p. 381-395.

12. Liao, X., Y. Shen, R. Zhang, K. Sugi, N.T. Vasudevan, M.A. Alaiti, D.R. Sweet, L. Zhou, Y. Qing, S.L. Gerson, C. Fu, A. Wynshaw-Boris, R. Hu, M.A. Schwartz, H. Fujioka, B. Richardson, M.J. Cameron, H. Hayashi, J.S. Stamler, and M.K. Jain (2018) Distinct roles of resident and nonresident macrophages in nonischemic cardiomyopathy. *Proc Natl Acad Sci U S A.* **115**(20): p. E4661-E4669.

13. Marinkovic, G., H. Grauen Larsen, T. Yndigegn, I.A. Szabo, R.G. Mares, L. de Camp, M. Weiland, L. Tomas, I. Goncalves, J. Nilsson, S. Jovinge, and A. Schiopu (2019) Inhibition of pro-inflammatory

468   myeloid cell responses by short-term S100A9 blockade improves cardiac function after
469   myocardial infarction. *Eur Heart J.* **40**(32): p. 2713-2723.

470   14.   Nahrendorf, M., F.K. Swirski, E. Aikawa, L. Stangenberg, T. Wurdinger, J.L. Figueiredo, P. Libby, R.
471   Weissleder, and M.J. Pittet (2007) The healing myocardium sequentially mobilizes two
472   monocyte subsets with divergent and complementary functions. *J Exp Med.* **204**(12): p. 3037-
473   3047.

474   15.   Patel, B., M.A. Ismahil, T. Hamid, S.S. Bansal, and S.D. Prabhu (2017) Mononuclear Phagocytes
475   Are Dispensable for Cardiac Remodeling in Established Pressure-Overload Heart Failure. *PLoS*
476   *One.* **12**(1): p. e0170781.

477   16.   Sager, H.B., M. Hulsmans, K.J. Lavine, M.B. Moreira, T. Heidt, G. Courties, Y. Sun, Y. Iwamoto, B.
478   Tricot, O.F. Khan, J.E. Dahlman, A. Borodovsky, K. Fitzgerald, D.G. Anderson, R. Weissleder, P.
479   Libby, F.K. Swirski, and M. Nahrendorf (2016) Proliferation and Recruitment Contribute to
480   Myocardial Macrophage Expansion in Chronic Heart Failure. *Circ Res.* **119**(7): p. 853-864.

481   17.   Weisheit, C., Y. Zhang, A. Faron, O. Kopke, G. Weisheit, A. Steinstrasser, S. Frede, R. Meyer, O.
482   Boehm, A. Hoeft, C. Kurts, and G. Baumgarten (2014) Ly6C(low) and not Ly6C(high)
483   macrophages accumulate first in the heart in a model of murine pressure-overload. *PLoS One.*
484   **9**(11): p. e112710.

485   18.   Bajpai, G., C. Schneider, N. Wong, A. Bredemeyer, M. Hulsmans, M. Nahrendorf, S. Epelman, D.
486   Kreisel, Y. Liu, A. Itoh, T.S. Shankar, C.H. Selzman, S.G. Drakos, and K.J. Lavine (2018) The human
487   heart contains distinct macrophage subsets with divergent origins and functions. *Nat Med.*
488   **24**(8): p. 1234-1245.

489   19.   Weinberger, T. and C. Schulz (2015) Myocardial infarction: a critical role of macrophages in
490   cardiac remodeling. *Front Physiol.* **6**: p. 107.

491   20.   Halade, G.V., V. Kain, and K.A. Ingle (2018) Heart functional and structural compendium of
492   cardiosplenic and cardiorenal networks in acute and chronic heart failure pathology. *Am J*
493   *Physiol Heart Circ Physiol.* **314**(2): p. H255-H267.

494   21.   Martini, E., P. Kunderfranco, C. Peano, P. Carullo, M. Cremonesi, T. Schorn, R. Carriero, A.
495   Termanini, F.S. Colombo, E. Jachetti, C. Panico, G. Faggian, A. Fumero, L. Torracca, M. Molgora, J.
496   Cibella, C. Pagiatakis, J. Brummelman, G. Alvisi, E.M.C. Mazza, M.P. Colombo, E. Lugli, G.
497   Condorelli, and M. Kallikourdis (2019) Single-Cell Sequencing of Mouse Heart Immune Infiltrate
498   in Pressure Overload-Driven Heart Failure Reveals Extent of Immune Activation. *Circulation.*
499   **140**(25): p. 2089-2107.

500   22.   Ma, Y., A. Yabluchanskiy, R.P. Iyer, P.L. Cannon, E.R. Flynn, M. Jung, J. Henry, C.A. Cates, K.Y.
501   Deleon-Pennell, and M.L. Lindsey (2016) Temporal neutrophil polarization following myocardial
502   infarction. *Cardiovasc Res.* **110**(1): p. 51-61.

503   23.   Horckmans, M., L. Ring, J. Duchene, D. Santovito, M.J. Schloss, M. Drechsler, C. Weber, O.
504   Soehnlein, and S. Steffens (2017) Neutrophils orchestrate post-myocardial infarction healing by
505   polarizing macrophages towards a reparative phenotype. *Eur Heart J.* **38**(3): p. 187-197.

506   24.   Lindsey, M.L., J.J. Saucerman, and K.Y. DeLeon-Pennell (2016) Knowledge gaps to understanding
507   cardiac macrophage polarization following myocardial infarction. *Biochim Biophys Acta.*
508   **1862**(12): p. 2288-2292.

509   25.   Ran, J., H. Qiu, S. Sun, A. Yang, and L. Tian (2018) Are ambient volatile organic compounds
510   environmental stressors for heart failure? *Environ Pollut.* **242**(Pt B): p. 1810-1816.

511   26.   Bennett, O., N.B. Kandala, C. Ji, J. Linnane, and A. Clarke (2014) Spatial variation of heart failure
512   and air pollution in Warwickshire, UK: an investigation of small scale variation at the ward-level.
513   *BMJ Open.* **4**(12): p. e006028.

514   27.   Tsai, D.H., J.L. Wang, K.J. Chuang, and C.C. Chan (2010) Traffic-related air pollution and
515   cardiovascular mortality in central Taiwan. *Sci Total Environ.* **408**(8): p. 1818-1823.

28. Villeneuve, P.J., M. Jerrett, J. Su, R.T. Burnett, H. Chen, J. Brook, A.J. Wheeler, S. Cakmak, and M.S. Goldberg (2013) A cohort study of intra-urban variations in volatile organic compounds and mortality, Toronto, Canada. *Environ Pollut.* **183**: p. 30-39.

29. Baba, S.P., D. Zhang, M. Singh, S. Dassanayaka, Z. Xie, G. Jagatheesan, J. Zhao, V.K. Schmidtke, K.R. Brittian, M.L. Merchant, D.J. Conklin, S.P. Jones, and A. Bhatnagar (2018) Deficiency of aldose reductase exacerbates early pressure overload-induced cardiac dysfunction and autophagy in mice. *J Mol Cell Cardiol.* **118**: p. 183-192.

30. Lang, A.L., L. Chen, G.D. Poff, W.X. Ding, R.A. Barnett, G.E. Arteel, and J.I. Beier (2018) Vinyl chloride dysregulates metabolic homeostasis and enhances diet-induced liver injury in mice. *Hepatol Commun.* **2**(3): p. 270-284.

31. Dassanayaka, S., Y. Zheng, A.A. Gibb, T.D. Cummins, L.A. McNally, K.R. Brittian, G. Jagatheesan, T.N. Audam, B.W. Long, R.E. Brainard, S.P. Jones, and B.G. Hill (2018) Cardiac-specific overexpression of aldehyde dehydrogenase 2 exacerbates cardiac remodeling in response to pressure overload. *Redox Biol.* **17**: p. 440-449.

32. An, O., K.T. Tan, Y. Li, J. Li, C.S. Wu, B. Zhang, L. Chen, and H. Yang (2020) CSI NGS Portal: An Online Platform for Automated NGS Data Analysis and Sharing. *Int J Mol Sci.* **21**(11).

33. Watson, L.J., H.T. Facundo, G.A. Ngoh, M. Ameen, R.E. Brainard, K.M. Lemma, B.W. Long, S.D. Prabhu, Y.T. Xuan, and S.P. Jones (2010) O-linked beta-N-acetylglucosamine transferase is indispensable in the failing heart. *Proc Natl Acad Sci U S A.* **107**(41): p. 17797-17802.

34. Watson, L.J., B.W. Long, A.M. DeMartino, K.R. Brittian, R.D. Readnower, R.E. Brainard, T.D. Cummins, L. Annamalai, B.G. Hill, and S.P. Jones (2014) Cardiomyocyte Ogt is essential for postnatal viability. *Am J Physiol Heart Circ Physiol.* **306**(1): p. H142-153.

35. Swamydas, M., Y. Luo, M.E. Dorf, and M.S. Lionakis (2015) Isolation of Mouse Neutrophils. *Curr Protoc Immunol.* **110**: p. 3 20 21-23 20 15.

36. Wilhelmsen, K., K. Farrar, and J. Hellman (2013) Quantitative in vitro assay to measure neutrophil adhesion to activated primary human microvascular endothelial cells under static conditions. *J Vis Exp.* 2013/09/03(78): p. e50677.

37. Swirski, F.K. and M. Nahrendorf (2018) Cardioimmunology: the immune system in cardiac homeostasis and disease. *Nat Rev Immunol.* **18**(12): p. 733-744.

38. Silvestre-Roig, C., Q. Braster, A. Ortega-Gomez, and O. Soehnlein (2020) Neutrophils as regulators of cardiovascular inflammation. *Nat Rev Cardiol.* **17**(6): p. 327-340.

39. Wang, Y., S. Sano, K. Oshima, M. Sano, Y. Watanabe, Y. Katanasaka, Y. Yura, C. Jung, A. Anzai, F.K. Swirski, N. Gokce, and K. Walsh (2019) Wnt5a-Mediated Neutrophil Recruitment Has an Obligatory Role in Pressure Overload-Induced Cardiac Dysfunction. *Circulation.* **140**(6): p. 487-499.

40. Frangogiannis, N.G. (2017) The extracellular matrix in myocardial injury, repair, and remodeling. *J Clin Invest.* **127**(5): p. 1600-1612.

41. Hutchinson, K.R., J.A. Stewart, Jr., and P.A. Lucchesi (2010) Extracellular matrix remodeling during the progression of volume overload-induced heart failure. *J Mol Cell Cardiol.* **48**(3): p. 564-569.

42. Salvador, A.M., T. Nevers, F. Velazquez, M. Aronovitz, B. Wang, A. Abadia Molina, I.Z. Jaffe, R.H. Karas, R.M. Blanton, and P. Alcaide (2016) Intercellular Adhesion Molecule 1 Regulates Left Ventricular Leukocyte Infiltration, Cardiac Remodeling, and Function in Pressure Overload-Induced Heart Failure. *J Am Heart Assoc.* **5**(3): p. e003126.

43. Bliksoen, M., L.H. Mariero, M.K. Torp, A. Baysa, K. Ytrehus, F. Haugen, I. Seljeflot, J. Vaage, G. Valen, and K.O. Stenslokken (2016) Extracellular mtDNA activates NF-kappaB via toll-like receptor 9 and induces cell death in cardiomyocytes. *Basic Res Cardiol.* **111**(4): p. 42.

17

563   44.   Lipps, C., J.H. Nguyen, L. Pyttel, T.L.t. Lynch, C. Liebetrau, G. Aleshcheva, S. Voss, O. Dorr, H.M.
564   Nef, H. Mollmann, C.W. Hamm, S. Sadayappan, and C. Troidl (2016) N-terminal fragment of
565   cardiac myosin binding protein-C triggers pro-inflammatory responses in vitro. *J Mol Cell Cardiol.*
566   **99**: p. 47-56.
567   45.   Krysko, D.V., P. Agostinis, O. Krysko, A.D. Garg, C. Bachert, B.N. Lambrecht, and P. Vandenabeele
568   (2011) Emerging role of damage-associated molecular patterns derived from mitochondria in
569   inflammation. *Trends Immunol.* **32**(4): p. 157-164.
570   46.   Shioi, T., A. Matsumori, Y. Kihara, M. Inoko, K. Ono, Y. Iwanaga, T. Yamada, A. Iwasaki, K.
571   Matsushima, and S. Sasayama (1997) Increased expression of interleukin-1 beta and monocyte
572   chemotactic and activating factor/monocyte chemoattractant protein-1 in the hypertrophied
573   and failing heart with pressure overload. *Circ Res.* **81**(5): p. 664-671.
574   47.   Patel, B., S.S. Bansal, M.A. Ismahil, T. Hamid, G. Rokosh, M. Mack, and S.D. Prabhu (2018)
575   CCR2(+) Monocyte-Derived Infiltrating Macrophages Are Required for Adverse Cardiac
576   Remodeling During Pressure Overload. *JACC Basic Transl Sci.* **3**(2): p. 230-244.
577   48.   Vandal, K., P. Rouleau, A. Boivin, C. Ryckman, M. Talbot, and P.A. Tessier (2003) Blockade of
578   S100A8 and S100A9 suppresses neutrophil migration in response to lipopolysaccharide. *J
579   Immunol.* **171**(5): p. 2602-2609.
580   49.   Ryckman, C., K. Vandal, P. Rouleau, M. Talbot, and P.A. Tessier (2003) Proinflammatory activities
581   of S100: proteins S100A8, S100A9, and S100A8/A9 induce neutrophil chemotaxis and adhesion.
582   *J Immunol.* **170**(6): p. 3233-3242.
583   50.   Morrow, D.A., Y. Wang, K. Croce, M. Sakuma, M.S. Sabatine, H. Gao, A.D. Pradhan, A.M. Healy, J.
584   Buros, C.H. McCabe, P. Libby, C.P. Cannon, E. Braunwald, and D.I. Simon (2008) Myeloid-related
585   protein 8/14 and the risk of cardiovascular death or myocardial infarction after an acute
586   coronary syndrome in the Pravastatin or Atorvastatin Evaluation and Infection Therapy:
587   Thrombolysis in Myocardial Infarction (PROVE IT-TIMI 22) trial. *Am Heart J.* **155**(1): p. 49-55.
588   51.   Healy, A.M., M.D. Pickard, A.D. Pradhan, Y. Wang, Z. Chen, K. Croce, M. Sakuma, C. Shi, A.C.
589   Zago, J. Garasic, A.I. Damokosh, T.L. Dowie, L. Poisson, J. Lillie, P. Libby, P.M. Ridker, and D.I.
590   Simon (2006) Platelet expression profiling and clinical validation of myeloid-related protein-14
591   as a novel determinant of cardiovascular events. *Circulation.* **113**(19): p. 2278-2284.
592   52.   Ichikawa, M., R. Williams, L. Wang, T. Vogl, and G. Srikrishna (2011) S100A8/A9 activate key
593   genes and pathways in colon tumor progression. *Mol Cancer Res.* **9**(2): p. 133-148.
594   53.   Buonafine, M., E. Martinez-Martinez, C. Amador, B. Gravez, J. Ibarrola, A. Fernandez-Celis, S. El
595   Moghrabi, P. Rossignol, N. Lopez-Andres, and F. Jaisser (2018) Neutrophil Gelatinase-Associated
596   Lipocalin from immune cells is mandatory for aldosterone-induced cardiac remodeling and
597   inflammation. *J Mol Cell Cardiol.* **115**: p. 32-38.
598   54.   Marques, F.Z., P.R. Prestes, S.G. Byars, S.C. Ritchie, P. Wurtz, S.K. Patel, S.A. Booth, I. Rana, Y.
599   Minoda, S.P. Berzins, C.L. Curl, J.R. Bell, B. Wai, P.M. Srivastava, A.J. Kangas, P. Soininen, S.
600   Ruohonen, M. Kahonen, T. Lehtimaki, E. Raitoharju, A. Havulinna, M. Perola, O. Raitakari, V.
601   Salomaa, M. Ala-Korpela, J. Kettunen, M. McGlynn, J. Kelly, M.E. Wlodek, P.A. Lewandowski,
602   L.M. Delbridge, L.M. Burrell, M. Inouye, S.B. Harrap, and F.J. Charchar (2017) Experimental and
603   Human Evidence for Lipocalin-2 (Neutrophil Gelatinase-Associated Lipocalin [NGAL]) in the
604   Development of Cardiac Hypertrophy and heart failure. *J Am Heart Assoc.* **6**(6).
605   55.   Yndestad, A., T. Ueland, E. Oie, G. Florholmen, B. Halvorsen, H. Attramadal, S. Simonsen, S.S.
606   Froland, L. Gullestad, G. Christensen, J.K. Damas, and P. Aukrust (2004) Elevated levels of activin
607   A in heart failure: potential role in myocardial remodeling. *Circulation.* **109**(11): p. 1379-1385.
608   56.   Yan, L., N. Borregaard, L. Kjeldsen, and M.A. Moses (2001) The high molecular weight urinary
609   matrix metalloproteinase (MMP) activity is a complex of gelatinase B/MMP-9 and neutrophil

610   gelatinase-associated lipocalin (NGAL). Modulation of MMP-9 activity by NGAL. *J Biol Chem.*
611   **276**(40): p. 37258-37265.

612   57.   Nuntagowat, C., K. Leelawat, and R. Tohtong (2010) NGAL knockdown by siRNA in human
613   cholangiocarcinoma cells suppressed invasion by reducing NGAL/MMP-9 complex formation.
614   *Clin Exp Metastasis.* **27**(5): p. 295-305.

615   58.   Boyd, J.H., B. Kan, H. Roberts, Y. Wang, and K.R. Walley (2008) S100A8 and S100A9 mediate
616   endotoxin-induced cardiomyocyte dysfunction via the receptor for advanced glycation end
617   products. *Circ Res.* **102**(10): p. 1239-1246.

618   59.   Tang, W.H., M.L. Brennan, K. Philip, W. Tong, S. Mann, F. Van Lente, and S.L. Hazen (2006)
619   Plasma myeloperoxidase levels in patients with chronic heart failure. *Am J Cardiol.* **98**(6): p. 796-
620   799.

621   60.   Ali, M., B. Pulli, G. Courties, B. Tricot, M. Sebas, Y. Iwamoto, I. Hilgendorf, S. Schob, A. Dong, W.
622   Zheng, A. Skoura, A. Kalgukar, C. Cortes, R. Ruggeri, F.K. Swirski, M. Nahrendorf, L. Buckbinder,
623   and J.W. Chen (2016) Myeloperoxidase Inhibition Improves Ventricular Function and
624   Remodeling After Experimental Myocardial Infarction. *JACC Basic Transl Sci.* **1**(7): p. 633-643.

625   61.   Griffith, J.W., C.L. Sokol, and A.D. Luster (2014) Chemokines and chemokine receptors:
626   positioning cells for host defense and immunity. *Annu Rev Immunol.* **32**: p. 659-702.

627   62.   Miyake, M., S. Goodison, V. Urquidi, E. Gomes Giacoia, and C.J. Rosser (2013) Expression of
628   CXCL1 in human endothelial cells induces angiogenesis through the CXCR2 receptor and the
629   ERK1/2 and EGF pathways. *Lab Invest.* **93**(7): p. 768-778.

630   63.   Scapini, P., M. Morini, C. Tecchio, S. Minghelli, E. Di Carlo, E. Tanghetti, A. Albini, C. Lowell, G.
631   Berton, D.M. Noonan, and M.A. Cassatella (2004) CXCL1/macrophage inflammatory protein-2-
632   induced angiogenesis in vivo is mediated by neutrophil-derived vascular endothelial growth
633   factor-A. *J Immunol.* **172**(8): p. 5034-5040.

634   64.   Wang, L., Y.L. Zhang, Q.Y. Lin, Y. Liu, X.M. Guan, X.L. Ma, H.J. Cao, Y. Liu, J. Bai, Y.L. Xia, J. Du, and
635   H.H. Li (2018) CXCL1-CXCR2 axis mediates angiotensin II-induced cardiac hypertrophy and
636   remodelling through regulation of monocyte infiltration. *Eur Heart J.* **39**(20): p. 1818-1831.

637   65.   Gillis, B., I.M. Gavin, Z. Arbieva, S.T. King, S. Jayaraman, and B.S. Prabhakar (2007) Identification
638   of human cell responses to benzene and benzene metabolites. *Genomics.* **90**(3): p. 324-333.

639   66.   Bironaite, D., D. Siegel, J.L. Moran, B.B. Weksler, and D. Ross (2004) Stimulation of endothelial
640   IL-8 (eIL-8) production and apoptosis by phenolic metabolites of benzene in HL-60 cells and
641   human bone marrow endothelial cells. *Chem Biol Interact.* **149**(2-3): p. 177-188.

642   67.   Gerszten, R.E., E.A. Garcia-Zepeda, Y.C. Lim, M. Yoshida, H.A. Ding, M.A. Gimbrone, Jr., A.D.
643   Luster, F.W. Luscinskas, and A. Rosenzweig (1999) MCP-1 and IL-8 trigger firm adhesion of
644   monocytes to vascular endothelium under flow conditions. *Nature.* **398**(6729): p. 718-723.

645   68.   Gomez-Pastor, R., E.T. Burchfiel, and D.J. Thiele (2018) Regulation of heat shock transcription
646   factors and their roles in physiology and disease. *Nat Rev Mol Cell Biol.* **19**(1): p. 4-19.

647   69.   Sakamoto, M., T. Minamino, H. Toko, Y. Kayama, Y. Zou, M. Sano, E. Takaki, T. Aoyagi, K. Tojo, N.
648   Tajima, A. Nakai, H. Aburatani, and I. Komuro (2006) Upregulation of heat shock transcription
649   factor 1 plays a critical role in adaptive cardiac hypertrophy. *Circ Res.* **99**(12): p. 1411-1418.

650   70.   Zhou, N., Y. Ye, X. Wang, B. Ma, J. Wu, L. Li, L. Wang, D.W. Wang, and Y. Zou (2017) Heat shock
651   transcription factor 1 protects against pressure overload-induced cardiac fibrosis via Smad3. *J*
652   *Mol Med (Berl).* **95**(4): p. 445-460.

653   71.   Du, P., Y. Chang, F. Dai, C. Wei, Q. Zhang, and J. Li (2018) Role of heat shock transcription factor
654   1(HSF1)-upregulated macrophage in ameliorating pressure overload-induced heart failure in
655   mice. *Gene.* **667**: p. 10-17.

656   72.   Zou, Y., J. Li, H. Ma, H. Jiang, J. Yuan, H. Gong, Y. Liang, A. Guan, J. Wu, L. Li, N. Zhou, Y. Niu, A.
657   Sun, A. Nakai, P. Wang, H. Takano, I. Komuro, and J. Ge (2011) Heat shock transcription factor 1

19

658   protects heart after pressure overload through promoting myocardial angiogenesis in male
659   mice. *J Mol Cell Cardiol.* **51**(5): p. 821-829.
660 73. Uchiyama, T., H. Atsuta, T. Utsugi, M. Oguri, A. Hasegawa, T. Nakamura, A. Nakai, M. Nakata, I.
661   Maruyama, H. Tomura, F. Okajima, S. Tomono, S. Kawazu, R. Nagai, and M. Kurabayashi (2007)
662   HSF1 and constitutively active HSF1 improve vascular endothelial function (heat shock proteins
663   improve vascular endothelial function). *Atherosclerosis.* **190**(2): p. 321-329.
664 74. Takii, R., S. Inouye, M. Fujimoto, T. Nakamura, T. Shinkawa, R. Prakasam, K. Tan, N. Hayashida,
665   H. Ichikawa, T. Hai, and A. Nakai (2010) Heat shock transcription factor 1 inhibits expression of
666   IL-6 through activating transcription factor 3. *J Immunol.* **184**(2): p. 1041-1048.
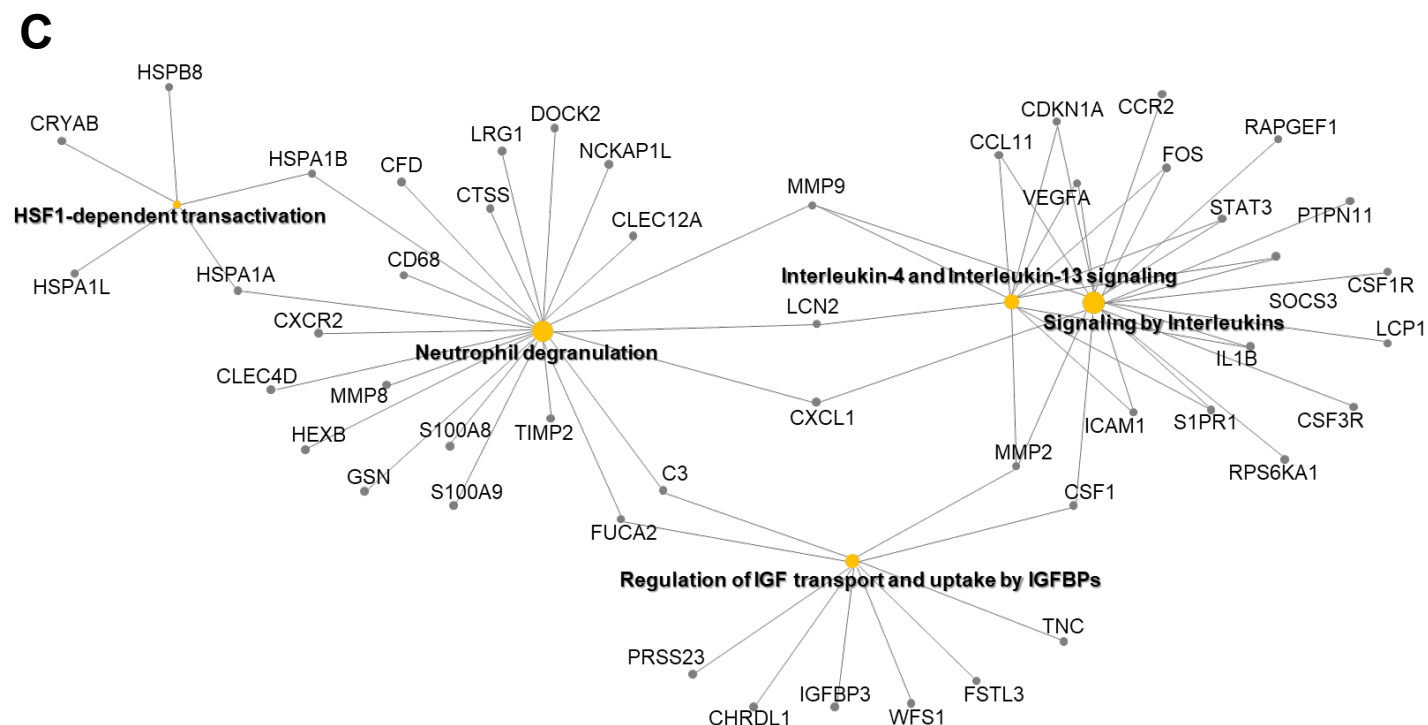667

Figure 1
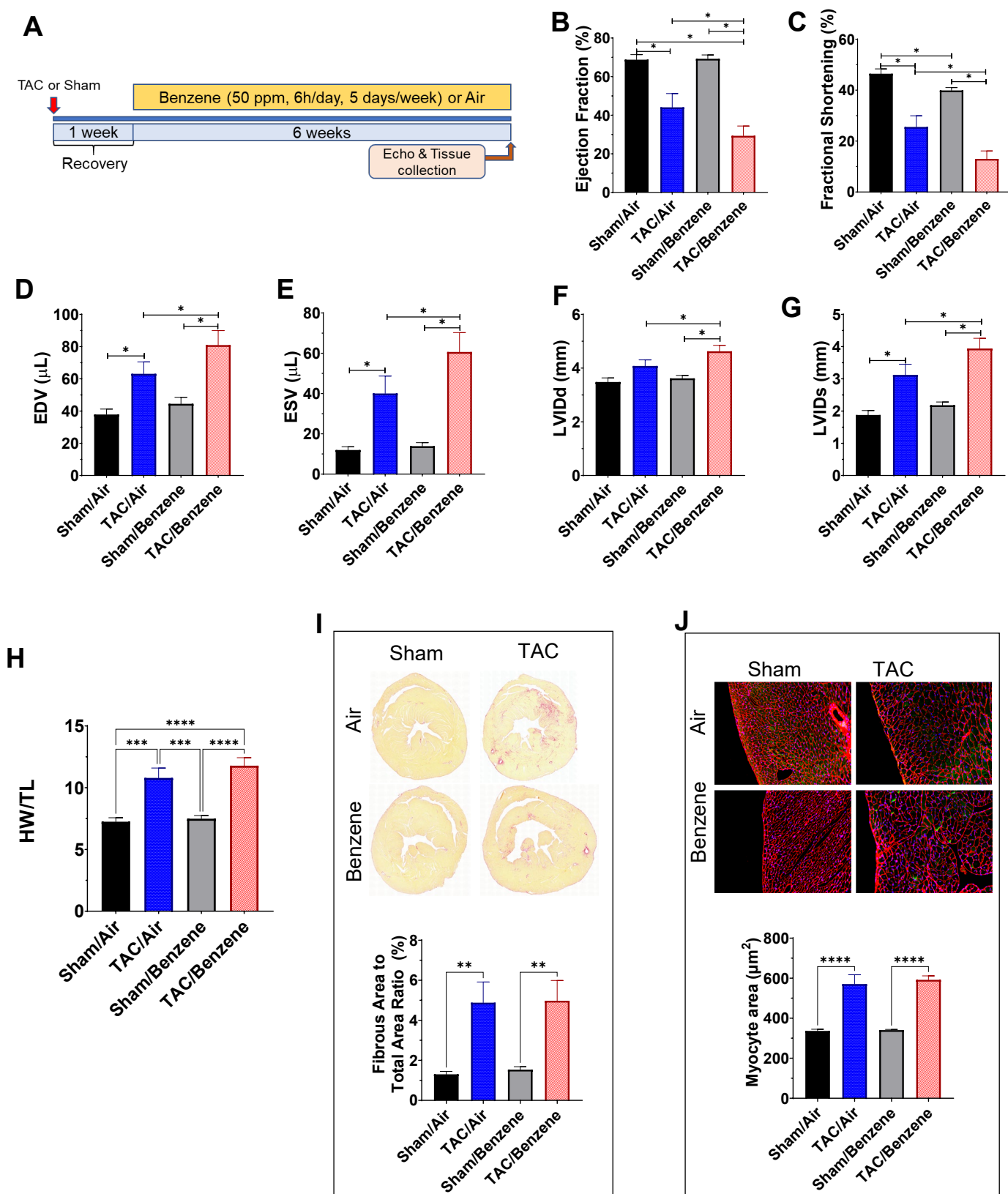
Figure 2
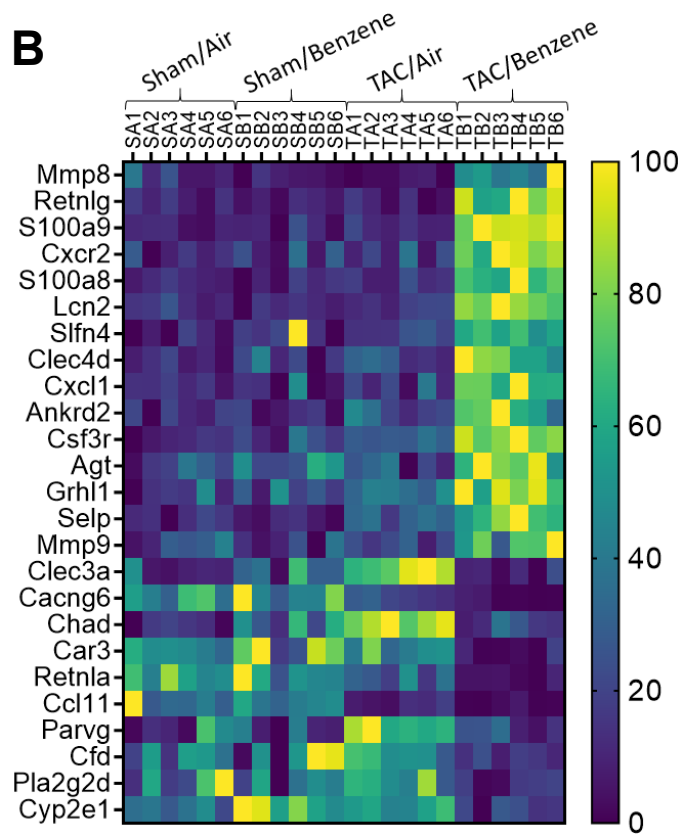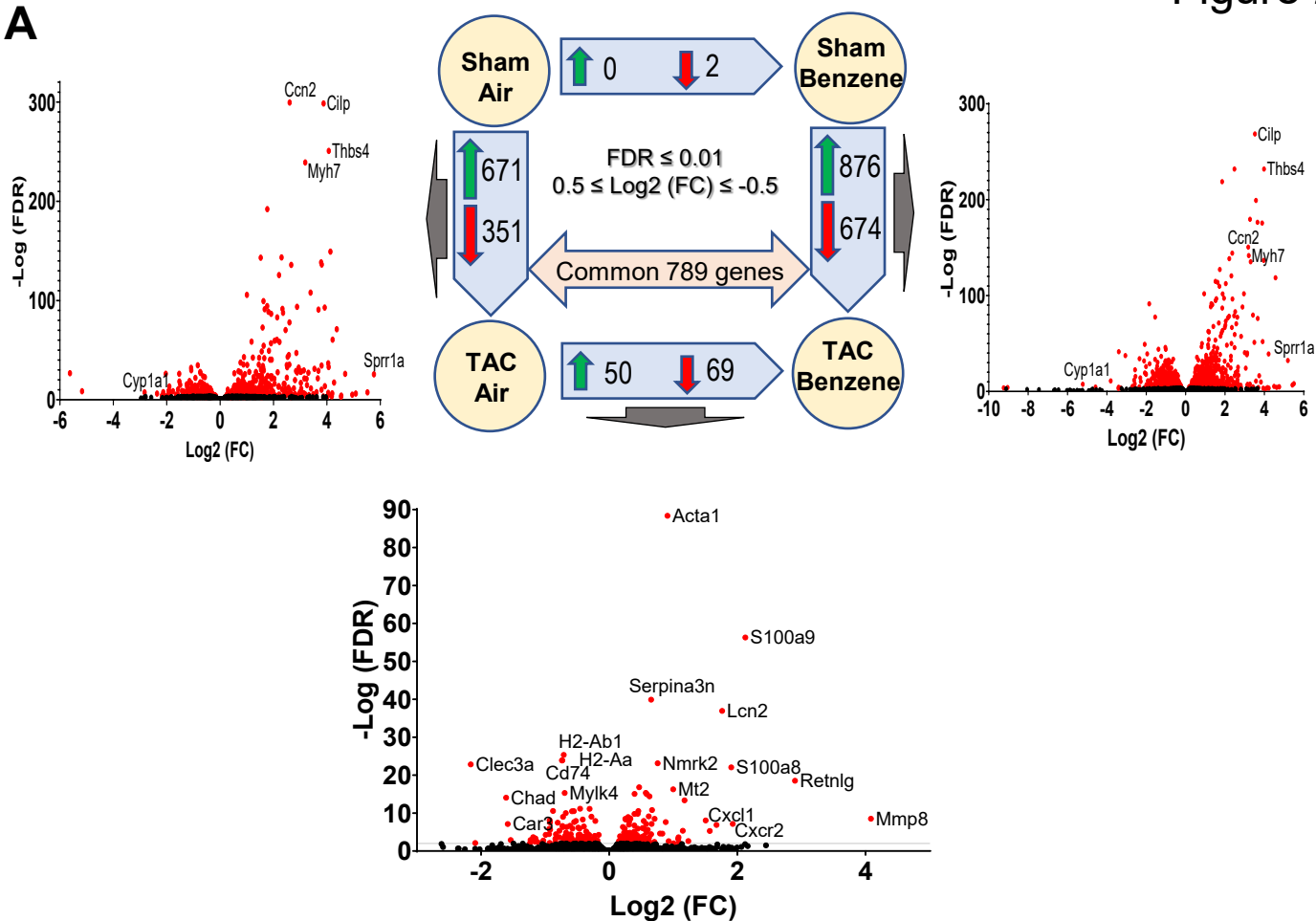
Figure 3

Figure 4

Figure 5

A

Selp relative mRNA levels

**

**

DMSO HQ Catechol

B

Control HQ Catechol

P-selectin

β-Actin

P-selectin/β-Actin

*

Control HQ Catechol

C

Relative adhesion (%)

*

****

Control HQ Catechol

D

Relative adhesion (%)

**

*

| HQ | - | + | + | - | - |
Catechol	-	-	-	+	+
Control IgG	-	+	-	+	-
CD62P IgG	-	-	+	-	+
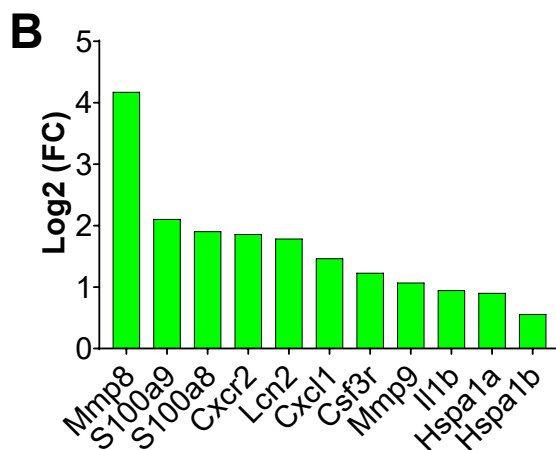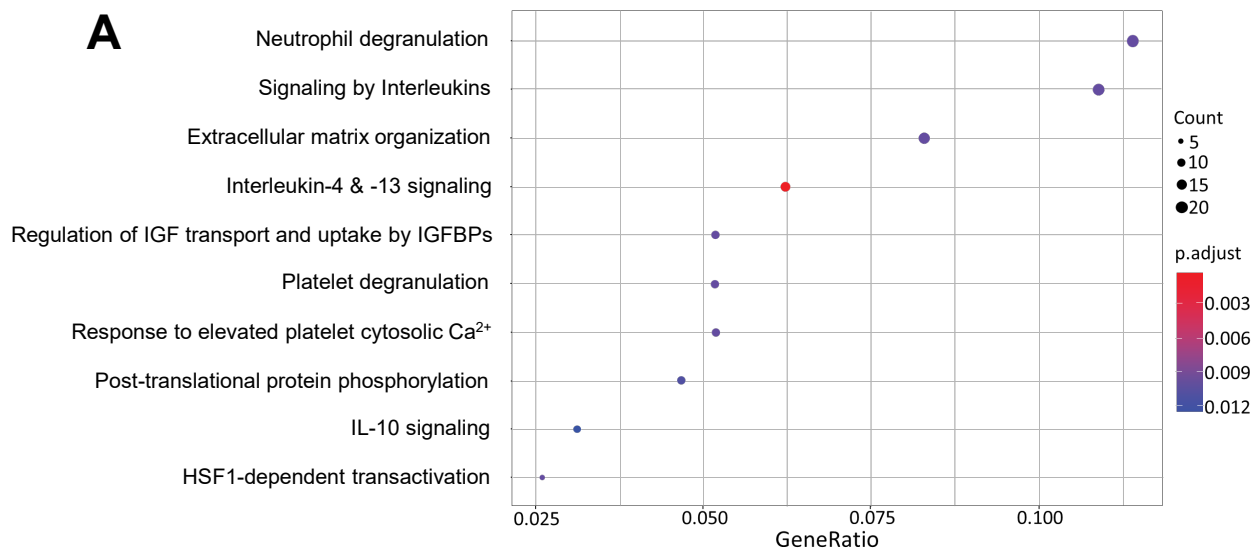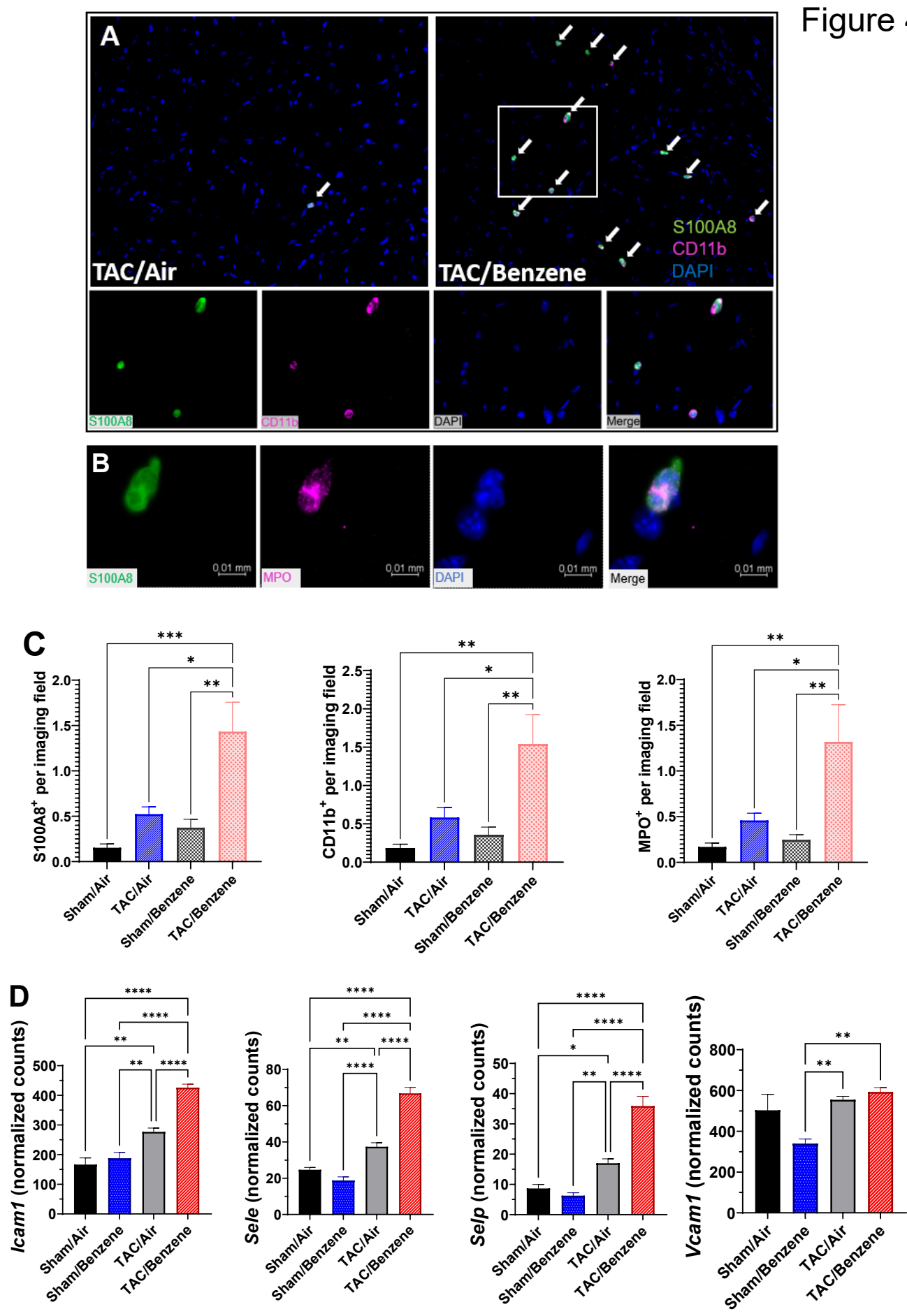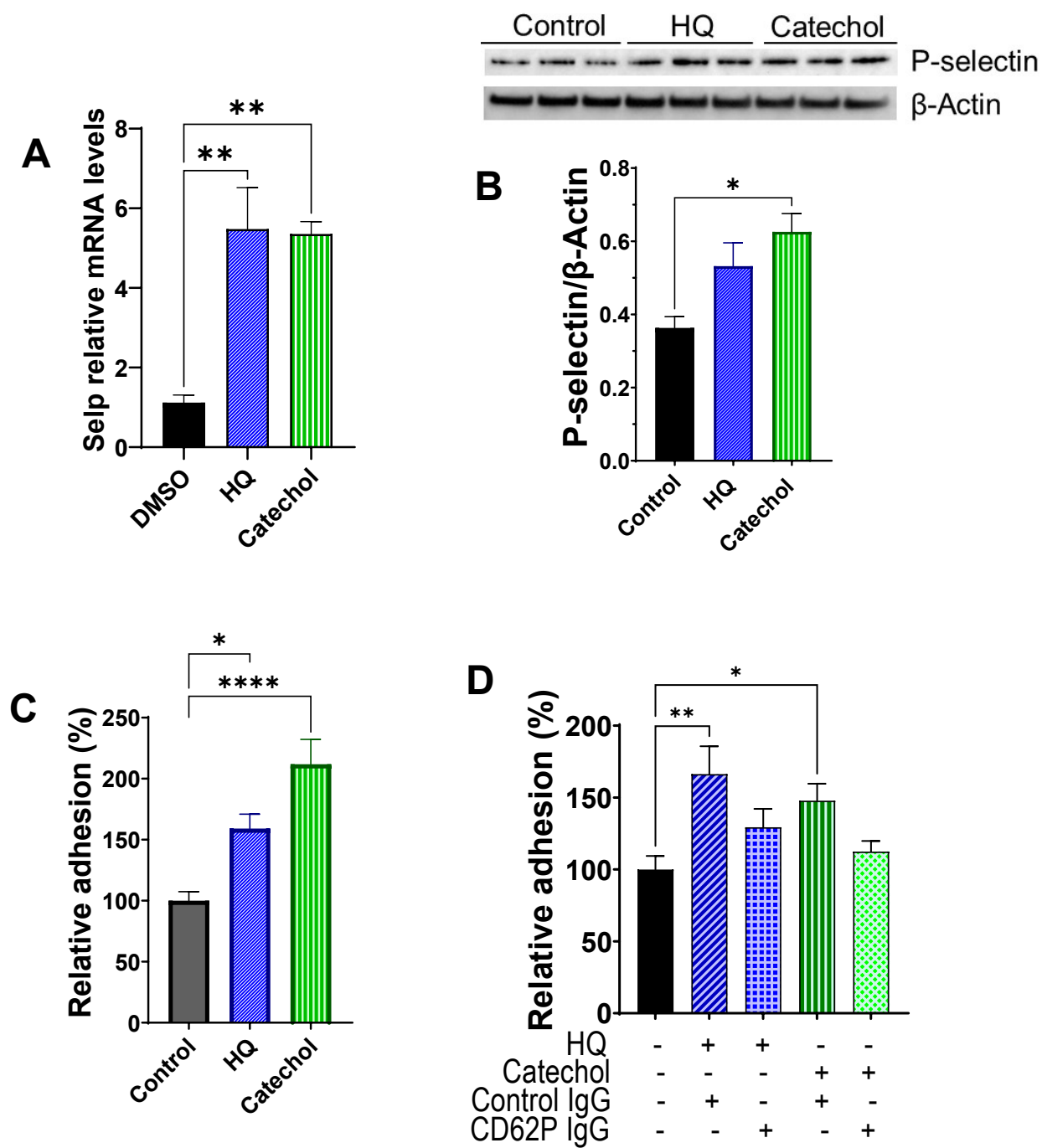
Supplementary Table 1. *Echocardiographic parameters of transverse aortic constriction or sham operated mice followed by benzene or air exposure for 6 weeks.*

| Parameters	Sham/Air	Sham/Benzene	TAC/Air	TAC/Benzene
IVRT (ms)	11.1 ± 0.6	12.6 ± 0.7	16.2 ± 2.0	17.8 ± 2.3*
LVAWd (mm)	1.3 ± 0.1	1.2 ± 0.03	$1.4 \pm 0.04^{\S}$	1.4 ± 0.07
LVAWs (mm)	1.9 ± 0.07	1.8 ± 0.04	1.8 ± 0.06	1.7 ± 0.09
LVPWd (mm)	1.1 ± 0.04	1.0 ± 0.05	$1.3 \pm 0.1^{\S}$	1.2 ± 0.06
LVPWs (mm)	1.8 ± 0.06	1.5 ± 0.06	1.6 ± 0.09	1.5 ± 0.09*
HR (bpm)	534 ± 11	514 ± 12	523 ± 9	549 ± 9
Endo CO (mL/min)	13.7 ± 1.01	15.6 ± 1.21	12.1 ± 0.98	$11.2 \pm 1.03^{\S}$
SV (µL)	25.9 ± 2.3	30.6 ± 2.7	23.1 ± 1.9	$20.3 \pm 1.7^{\S}$

Values are mean $\pm$ SEM. N=10-12 per group. *$p \leq 0.05$ vs Sham/Air, $^{\S}p \leq 0.05$ vs Sham/Benzene. Statistical analyses were performed by One-way ANOVA.
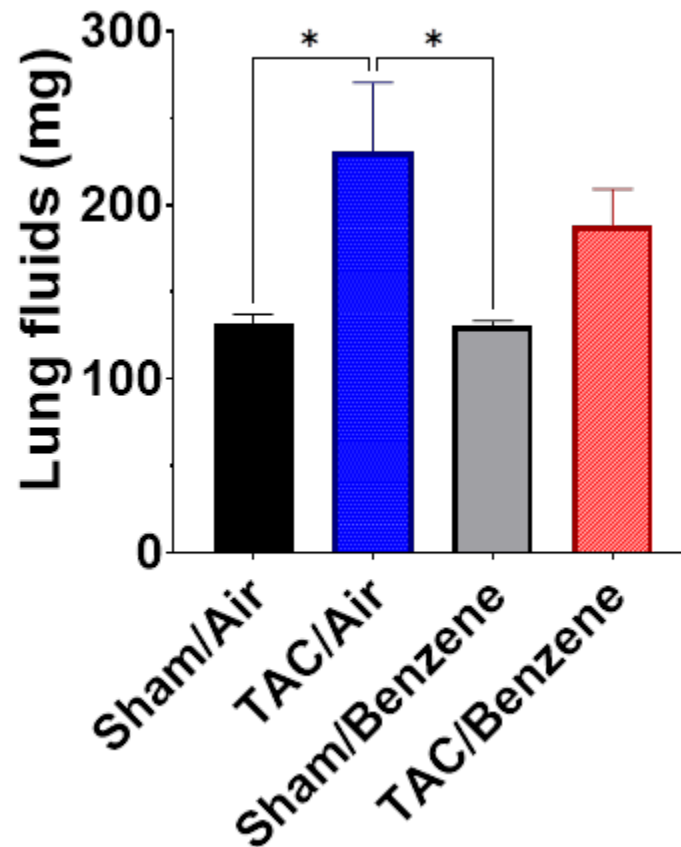
Supplementary Figure 1. *Pulmonary edema in transverse aortic constriction or Sham operated mice exposed to benzene or air for 6 weeks.* Accumulation of the fluid in the lung was measured by subtracting the dry weight of the tissue from the wet weight. Values are mean ± SEM, N=10-12 per group. *$p<0.05$ between corresponding groups. Statistical analyses were performed by One-way ANOVA.
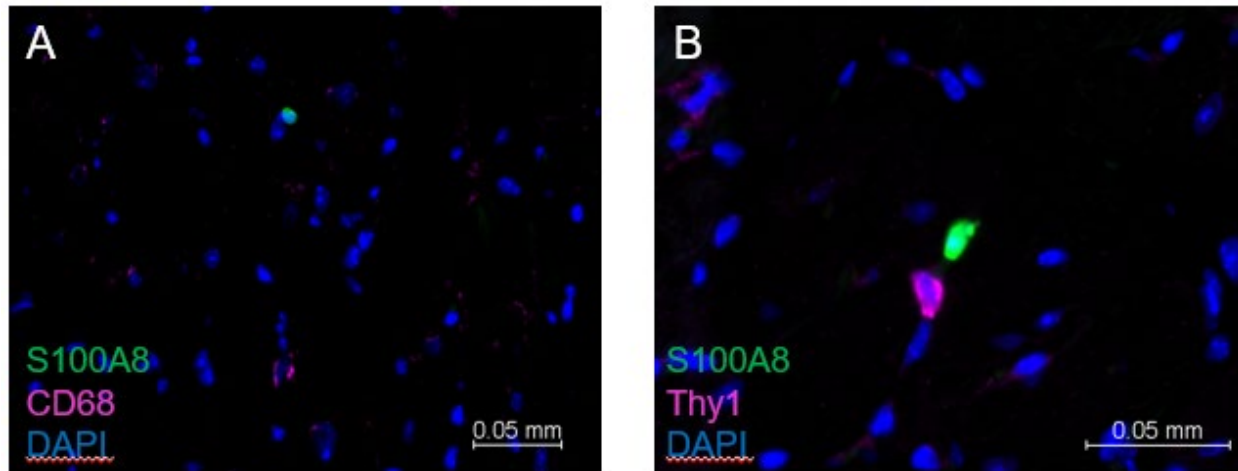
Supplementary Figure 2. *Staining of immune cells in the hearts of TAC/Benzene-exposed mice.* Hearts from the TAC/Benzene mice were stained with granulocyte marker S100A8, macrophage marker CD68, or fibroblast marker Thy1. Nuclei were stained with DAPI (blue).
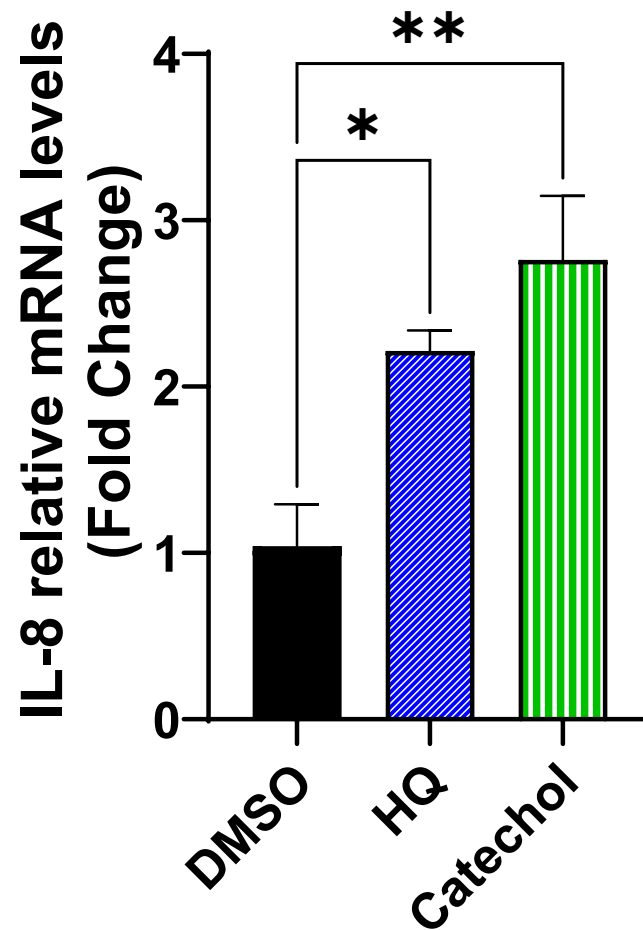
Supplementary Figure 3. Expression of chemokine IL8 in hydroquinone (HQ, 5 µM/24h) and catechol cardiac (5 µM/24h)-treated cardiac microvascular endothelial cells. Values are mean ± SEM, N=3 per group. *p<0.05, **p<0.01 between corresponding groups. Statistical analyses were performed by One-way ANOVA.